Iron oxidation state variations in zoned micro-crystals measured using micro-XANES

Iron oxidation state variations in zoned micro-crystals measured using micro-XANES

Lorenzo Mino[1], Elisa Borfecchia[1*], Chiara Groppo[2], Daniele Castelli[2], Gema Martinez Criado[3], Richard Spiess[4], Carlo Lamberti[1]

[1] Dept. of Chemistry, University of Turin, via Giuria 7, I-10125 Torino (Italy); NIS Centre of Excellence and INSTM Centro di Riferimento, via Quarello 11, I-10135, Torino (Italy)

[2] Dept. of Earth Sciences, University of Torino, via Valperga Caluso 35, I-10125 Torino (Italy)

[3] European Synchrotron Radiation Facility, ID22, 6, rue Jules Horowitz, B.P. 220, F-38043 Grenoble cedex (France)

[4] Dept. of Geoscience, University of Padova, Via Gradenigo 6, I-35131 Padova (Italy)

*elisa.borfecchia@unito.it

Abstract

The determination of the oxidation state of transition metals at high spatial resolution is a crucial issue for many fields of science, including solid state physics, earth sciences, biology, bio-chemistry and catalysis. Among the other available analytical methods, micro-XANES allows to probe *in situ* the oxidation state with high lateral resolution, enabling an unprecedented level of description in heterogeneous samples. In geological samples the determination of the $Fe^{3+}/\Sigma Fe$ ratio is of particular interest since it can be used as an indicator of the oxygen fugacity (fO_2) at which a mineral formed. With this respect, we performed a micro-XANES aiming to investigate the Fe-redox state variation across single-crystals of both garnet and omphacite exploiting the X-ray microprobe available at the ESRF ID22 beamline to reach a spot size of 1.7 μm × 5.3 μm. For garnet, the absolute Fe^{3+} content was determined in a space-resolved way. In the case of omphacite, the analysis of the XANES data is not straightforward owing to the presence of a significant dichroism effect and to the random orientation of the different grains in the mineral assemblage. The investigated samples are highly complex materials which represent a challenge for the micro-XANES technique. These zoned micro-crystals are therefore ideal systems to develop analytical procedures which

can be subsequently generalized to other relevant fields of science such as the Fe speciation in a single cell or a single grain for life science and catalysis applications, respectively.

Keywords

Fe oxidation state; micro-XANES; X-ray micro-beam; *in situ* characterization; zoned micro-crystals, polarization-dependent XANES

1 Introduction

The determination of the oxidation state of transition metals is a problem of primary importance for many fields of science, ranging from solid state physics to structural biology. X-ray Absorption Spectroscopy (XAS) is a powerful tool to address this issue since the analysis of the X-ray Absorption Near Edge Structure (XANES) region can simultaneously provide information on electronic and local structural properties.

Generally, XANES spectroscopy is performed using mm-sized X-ray beams, thus measuring absorption coefficients integrated over a relatively large volume [1]. However, in the last years the huge increase in the brightness of synchrotron radiation sources and the new developments in the X-rays focusing devices allowed to obtain intense (sub-)micron X-ray beams and to drastically improve the spatial resolution down to 10 nm [2]. The possibility to perform also XANES with high lateral resolution (micro-XANES) paved the way for a new level of description of heterogeneous samples or individual nanostructures [3, 4]. For instance, micro-XANES is probably the unique analytical method available to probe *in situ* the oxidation state of trace elements within cell and subcellular compartments [5, 6]. Interestingly, the two first studies that demonstrated the feasibility of micro-XANES on single cells were both devoted to the determination of Fe oxidation state [7, 8].

Also in the field of heterogeneous catalysis probing the structural and electronic properties of materials *in situ* is of central importance and in many cases spatial variations in catalyst structure can be crucial as in the case of microstructured catalysts or integral catalytic reactors with prominent concentration and temperature profiles [9-15]. For instance, de Smith *et al.* studied the Fe-based Fischer Tropsch Synthesis (FTS) catalyst by imaging an individual catalyst particle at a resolution of 35 nm using chemical micro-spectroscopy [16, 17]. Also Tada *et al.* investigated by Ni K-edge micro-XAS the oxidation state and local coordination

structure of a single particle of a practical catalyst $NiO_x/Ce_2Zr_2O_y$ using a 1.0 x 0.8 μm^2 beam [18]. Another relevant example is the study of the spatial changes of the catalyst oxidation state in a fixed-bed microreactor as a function of temperature and velocity of the reaction mixture performed by Grunwaldt *et al.* [10, 19]. The previously discussed studies adopted a scanning (sub-)micro-XAS mode: another possibility to obtain space resolved information on the element oxidation state is to use full-field transmission X-ray microscopy. This approach ensures larger field of views and faster acquisition times at sub-micrometric resolution, but cannot be used for trace elements detection and needs precise sample realignment after flat field acquisition [1, 2, 20, 21]. The same Fe-based FTS catalyst studied by de Smith *et al.* [16] using a scanning approach was recently investigated also by full-field transmission X-ray microscopy allowing the *in situ* 3D characterization of an individual particle with nanometer spatial resolution and elemental sensitivity under realistic reaction conditions [22].

Finally, micro-XANES has been widely employed for the space-resolved determination of ferric iron contents on micrometric crystals without destroying their textural context [23-30]. In geological samples the determination of the $Fe^{3+}/\Sigma Fe$ ratio is of particular interest since it can be used as an indicator of the oxygen fugacity (fO_2) at which a mineral formed. In particular, micro-scale measurements of the $Fe^{3+}/\Sigma Fe$ ratio in zoned crystals are essential to understand the variations in the redox conditions experienced by the mineral during its progressive growth in different geodynamic contexts (e.g. during subduction at high- to ultra-high pressures [26, 31] or at mantle depths [32]).

In this paper we present a micro-XANES study of the $Fe^{3+}/\Sigma Fe$ ratio spatial variations in two different minerals, garnet and omphacite, both occurring as strongly zoned micrometric crystals. The challenge of our investigation was threefold: (i) the $Fe^{3+}/\Sigma Fe$ variations across the zoned crystals are expected to be small (< 10%), therefore a high spectral resolution is needed to appreciate the differences in the oxidation state; (ii) the spatial resolution has to be in the order of microns since the $Fe^{3+}/\Sigma Fe$ variations are expected to occur on a micrometric scale; (iii) for omphacite, which crystallizes in the monoclinic system, the effect of the X-ray beam polarization has to be considered, as it can result in X-ray dichroism effects.

From the above mentioned issues, it clearly emerges that the investigated samples are highly complex materials which represent a challenge for the micro-XANES technique. These zoned micro-crystals are therefore ideal systems to develop analytical procedures which can be subsequently employed also for

different kinds of samples to measure *in situ* the iron oxidation state, relevant in the disciplines mentioned above: solid state physics, earth sciences, biology, bio-chemistry and catalysis.

2 Material and methods

2.1 Samples Description

The measured almandine ($Fe^{3+}/\Sigma Fe = 0$) and magnetite ($Fe^{3+}/\Sigma Fe = 2/3$) crystals are high purity reference standards for X-ray microanalysis (SPI Supplies – reference numbers: #AS1020-AB and #AS1210-AB), mounted in a 25 mm diameter, 6 mm thick non-magnetic stainless steel disc. The measured augite crystal ($Fe^{3+}/\Sigma Fe = 0$), well characterized at EMP-WDS (sample 5P104 [33]), belongs to a thin section of a marble from the Sesia Zone (western Alps), ca. 30 μm thick, mounted on a high chemical purity SiO_2 amorphous slide using Fe-free Araldit®-epoxy. The single crystal of aegirine ($Fe^{3+}/\Sigma Fe = 1$) characterized using micro-XANES is a high purity reference standard for X-ray microanalysis (sample H091 [33]) mounted in a 2 mm diameter, 10 mm thick non-magnetic stainless steel disc.

The investigated micro-crystals of garnet and omphacite belong to a fine-grained eclogite (from the Monviso meta-ophiolitic Massif, Italian western Alps), consisting of omphacite, garnet and rutile with minor blue amphibole and very minor lawsonite, talc and jadeite [34], petrologically interpreted by Groppo and Castelli [31]. The polished thin section (ca. 30 μm thick) is mounted on a high chemical purity SiO_2 amorphous slide using Fe-free Araldit®-epoxy. Garnet occurs as small idioblasts (up to 0.5 mm in diameter) set in a matrix mainly consisting of omphacite (up to 0.5 – 0.6 mm in length). Garnet cores are crowded of very small inclusions mostly of omphacite, whereas garnet rims are almost free of inclusions. Both SEM-EDS and EMP analytical techniques have been used to analyze the major element concentrations across garnet and omphacite crystals. The microphotographs of the analyzed garnet and omphacite micro-crystals are reported in Figure 1

Garnet is strongly zoned, showing a Mn and Ca decrease toward the rim, counterbalanced by a Fe and Mg increase. More in detail, the X_{Mn} decreases from 0.24 in the core to 0.00 in the rim and it is balanced by an increase in both X_{Mg} and X_{Fe} (X_{Mg} is 0.01 to 0.12, and X_{Fe} is 0.56 to 0.82 from core to rim, respectively). Ca zoning is more complex, slightly increasing from the inner core to the outer core and decreasing toward the rim (X_{Ca} varies from 0.21 to 0.27 and to 0.11 toward the rim [31]) [$X_{Mn} = Mn/(Ca+Mg+Fe^{2+}+Mn)$; $X_{Mg} =$

Mg/(Ca+Mg+Fe^{2+}+Mn); X_{Ca} = Ca/(Ca+Mg+Fe^{2+}+Mn); X_{Fe} = Fe^{2+}/(Ca+Mg+Fe^{2+}+Mn)].

Omphacite in the rock matrix is also strongly zoned: the deep green omphacite core (Omp_c in Figure 6b) has higher X_{Aeg} and lower X_{Jd} [X_{Aeg} = 35→28; X_{Jd} = 25→35; $X_{Mg}(Fe_{tot})$ = 40 – 50] than omphacite rim (Omp_r in Figure 6b) [X_{Aeg} = 24→14; X_{Jd} = 35→45; $X_{Mg}(Fe_{tot})$ = 52 – 66] [X_{Aeg} = Fe^{+3}/(Fe^{+3}+Al^{VI}+Fe^{+2}+Mg)×100; X_{Jd} = Al/(Fe^{+3}+Al^{VI}+ Fe^{+2}+Mg) ×100; $X_{Mg}(Fe_{tot})$ = Mg/(Mg+Fe)] [31].

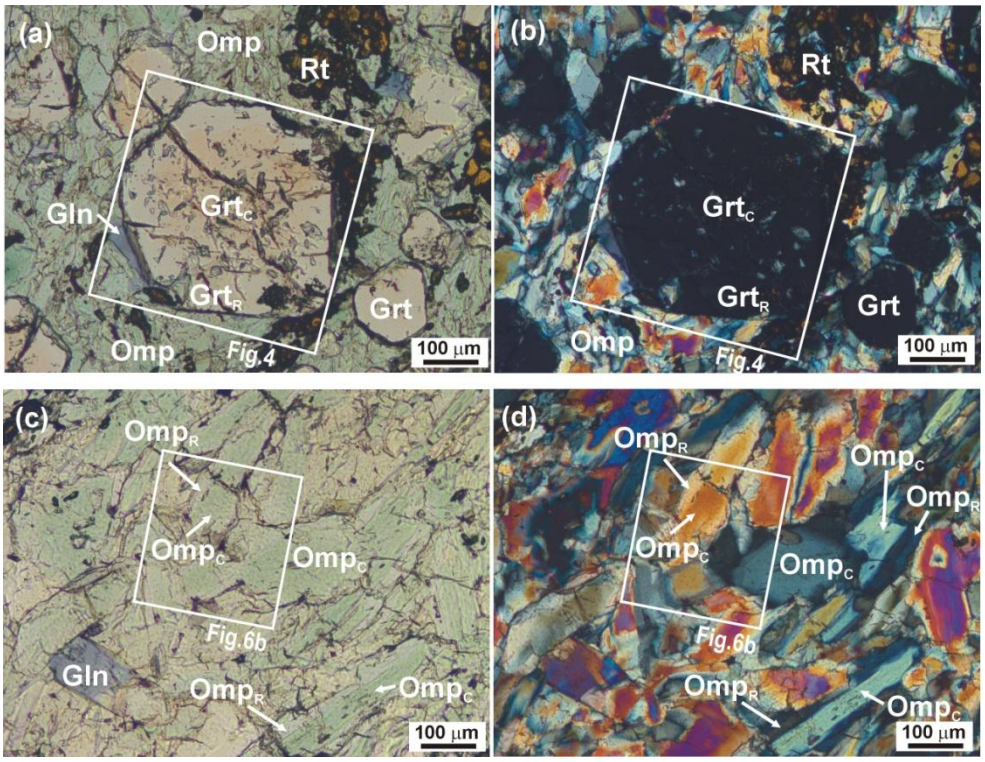

Figure 1. (a) Microphotograph in plane polarized light (PPL) of the analyzed garnet micro-crystal, set in a matrix composed of omphacite (Omp), rutile (Rt) and minor glaucophane (Gln). Garnet is strongly zoned, with a reddish core (GrtC) crowded of inclusions and a pinkish rim (GrtR). (b) As part (a) using crossed polarized light (XPL). (c) Microphotograph in PPL of the analyzed omphacite micro-crystals. Omphacite is zoned, with a darker green core (OmpC) and a lighter green rim (OmpR). (d) As part (c) using XPL. The white boxes highlight the micro-crystals investigated using micro-XANES spectroscopy (see Figure 4 for garnet and Figure 6b for omphacite).

2.2 Micro-XANES Spectroscopy

Fe K-edge XANES spectra were recorded at the ID22 beamline of the ESRF at Grenoble [35, 36] which exploits the radiation produced by two different undulators: a standard linear undulator (U42), covering the energy range from 6 to 50 keV, and a second one (U23), which is a so-called in-vacuum linear undulator, inducing a much higher brilliance. Harmonic rejection is done by a flat horizontally deflecting Si mirror. A

Kohzu fixed-exit double crystal monochromator with Si(311) crystals was employed in this work to ensure a better energy resolution (0.5 eV) compared to Si(111) crystals (1 eV).

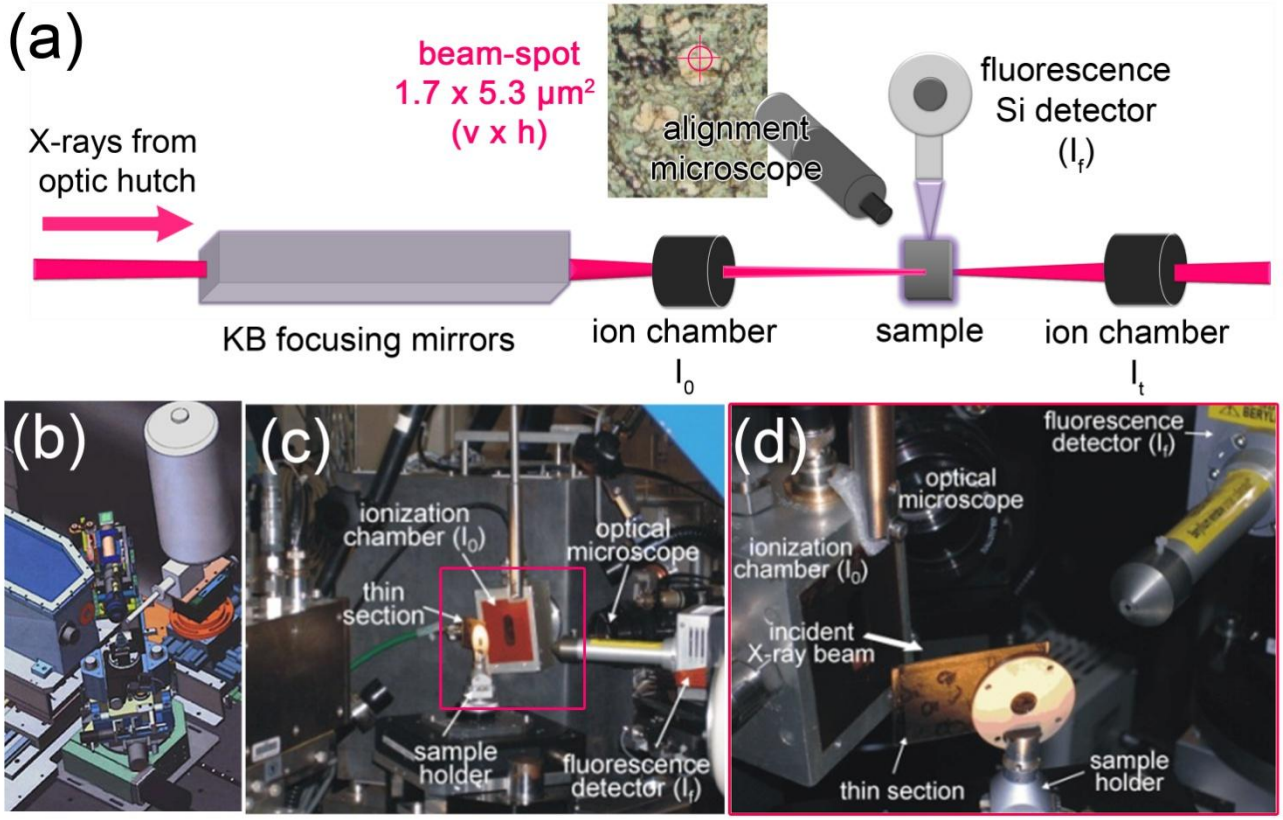

Figure 2. (a) Scheme of the experimental microprobe used at the ESRF ID22 beamline, containing the KB focusing mirrors, two ionization chambers to measure I_0 and I_t, the X-ray fluorescence detector (which during the acquisition is located at 90° respect to the X-ray beam to minimize Compton scattering), the rotating sample holder and the optical microscope for sample/beam alignment. (b) 3D scheme of the experimental set-up reported in part (a). (c-d) Photographs showing the details of the experimental set-up and the position of the sample.

The microprobe set-up is based on the Kirkpatrick-Baez (KB) mirrors [2], that allowed us to reach a beam size of 1.7 μm (vertical) × 5.3 μm (horizontal). The focused beam profiles were collected by means of knife-edge scans [37]. A gold cross deposited by electron beam lithography on a Si substrate is translated vertically and horizontally through the X-ray micro-beam using a well-calibrated piezo stage. Assuming a beam propagating with a Gaussian intensity profile, the beam sizes in both horizontal and vertical directions are estimated separately from the FWHM of the numerical derivative of the Au fluorescence intensity as a function of the position.

When the current on the ESRF ring is 200 mA, the KB mirrors, having an efficiency of approximately 70%,

allow to obtain in the focal spot a photon flux of about 10^{12} photon/s at 13 keV. As visible in Figure 2, different detectors such as a mini-ionization chamber and a Silicon Drift Detector are used to monitor the intensity of the incoming beam and the XRF signals. A video-microscope allows for the easy alignment of the sample and the microprobe set-up.

All XANES spectra were recorded in X-ray fluorescence mode. The samples were mounted at 45° with respect to both the incident beam and the Si drift detector (see Figure 2c-d). XANES spectra were recorded using a 2 eV step size for the far pre-edge region and a 0.1 eV step size in the pre-edge and edge regions (7105 – 7135 eV); in the post-edge region (from k = 1.6 $Å^{-1}$ to k = 10 $Å^{-1}$) a k-step of 0.05 $Å^{-1}$ was used. An integration time of 1 second per point was adopted in the whole range except for the region containing the features of interest (7111 – 7119 eV), where the integration time was increased to 5 seconds. The total scan time was 25 – 30 min. A precise calibration of the monochromator energy was carried out by measuring a reference XANES spectrum of a Fe foil (EXAFS Materials Inc.) in transmission geometry, and then defining the first derivative peak at the tabulated value of 7112.0 eV [38]. In order to precisely locate the microstructural sites of interest, different micro-XRF profiles were acquired on the garnet and omphacite micro-crystals.

The Athena software [39] was used for the extraction of the data. The edge jump was estimated fitting the far pre-edge region (E < 7105 eV) with a linear function, while the post edge was reproduced with a second order spline. Spectra were compared after normalization.

2.3 Electron Back-Scattered Diffraction

The crystallographic orientations of aegirine and augite used as Fe^{3+} and Fe^{2+} pyroxene end-members and those of the omphacite micro-crystals on which the micro-XANES spectra were acquired, were obtained using the electron back-scattered diffraction (EBSD) technique. The thin sections were polished using Syton fluid to remove the mechanical damage generated during previous mechanical polishing [40, 41]. After polishing, the samples were coated with a thin carbon film to prevent electrical charging problems. EBSD analysis was performed using a CamScan MX2500 SEM equipped with a tungsten filament at the Department of Geosciences, the University of Padova (Italy). An acceleration voltage of 25 kV, a filament emission current of 150 μA, and a working distance of 25 mm were used. EBSD patterns were indexed using CHANNEL 5.0 software from HKL-Technology. Indexing was accepted when at least five detected Kikuchi

bands corresponded with those contained in the standard reflector files for aegirine (for the aegirine crystal) and diopside (for augite and omphacite).

3 Results and Discussion

3.1 Cubic micro-crystals

In a XANES spectrum collected at the Fe K-edge, the pre-edge features which are located at ~10 – 20 eV before the edge jump (see Figure 3) are particularly sensitive to the iron oxidation state and therefore are usually monitored [26, 27, 42-47]. These features are related to 1s → 3d (quadrupolar) and to 1s → 4p (dipolar) electronic transitions [48] and, in general, their position shifts towards higher energy when increasing the oxidation state [43]. In a centrosymmetric environment only the weak electric quadrupole mechanism is allowed, whereas the electric dipole mechanism also contributes to the process if the iron is in a non-centrosymmetric site [48]. Indeed, a marked increase in intensity can occur as a result of the metal 3d-4p orbital mixing and metal 3d-ligand 2p-orbital overlap, which relax the forbidden character of the electric dipole transition.

Figure 3a shows as an example the Fe K-edge XANES spectra of two Fe-bearing minerals which crystallize in the cubic system. Almandine (space group: Ia3d) is one end-member of the garnet mineral solid solution series since it contains only 8-coordinated Fe^{2+}: its pre-edge feature can be fitted using two Gaussian components [43] and the corresponding pre-edge centroid energy position is 7113.0 eV. In magnetite (space group: Fd3m) the pre-edge features are considerably stronger owing to the presence of tetrahedrally coordinated Fe^{3+}: the lack of inversion symmetry gives rise to the local mixing of 3d and 4p states, implying a combination of the 1s → 3d quadrupole and 1s → 4p dipole transitions, as discussed above. Besides the main contribution related to tetrahedral Fe^{3+}, also two weaker shoulders, arising from Fe^{2+} and octahedrally coordinated Fe^{3+}, are present [43]. The pre-edge centroid energy position for magnetite is 7114.6 eV: as expected, this value is shifted to higher energies with respect to almandine owing to the higher average Fe oxidation state in magnetite ($Fe^{3+}/\Sigma Fe = 2/3$).

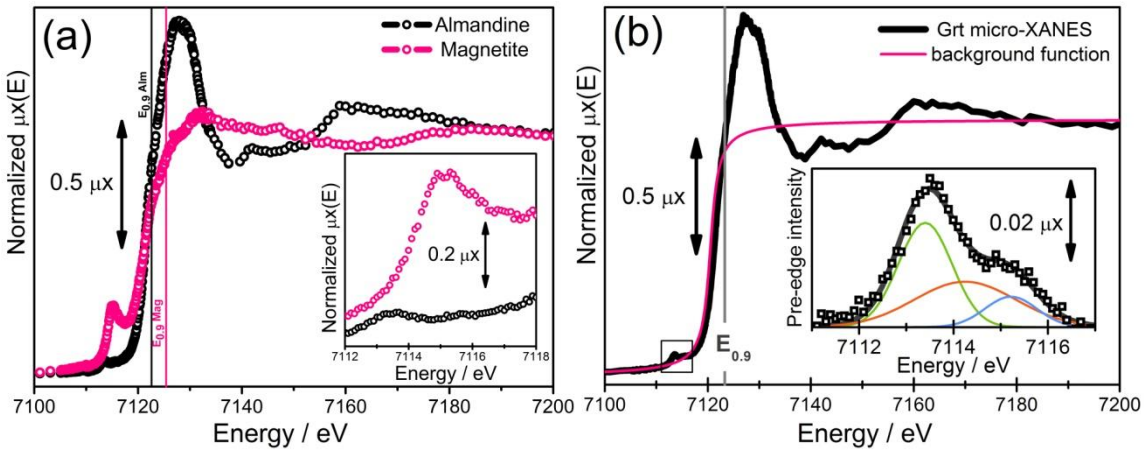

Figure 3. (a) Fe K-edge XANES spectra of almandine and magnetite. The $E_{0.9}$ position for the two samples is indicated by the vertical lines. In the inset a magnification of the pre-edge region is reported. (b) Fe K-edge XANES spectrum acquired in the garnet core (see Figure 4c). The simulated background is plotted as a magenta line; the E0.9 position is highlighted by the gray line. The inset shows the deconvolution of the pre-edge features using three Gaussian functions after background subtraction.

Previous studies on Fe-bearing minerals [49-51] and particularly on garnets, highlighted that the above described procedure, based on the pre-edge centroid energy position, which has been widely employed for the quantification of $Fe^{3+}/\Sigma Fe$ [26, 27, 42, 43, 45], is relatively insensitive to small variations of iron oxidation state at low values of $Fe^{3+}/\Sigma Fe$ [32], as expected in our garnet micro-crystal [31]. To confirm this observation, we acquired 20 micro-XANES spectra along the garnet micro-crystal (see SEM-EDS image in Figure 4c). The pre-edge features were fitted with three Gaussian functions (Figure 3b) and the centroid was calculated as the intensity-weighted average energy position of the maxima. Analyzing the energy positions of the pre-edge centroids reported in Figure 4a, we can conclude that it is not possible to identify clear differences in the centroid positions along the garnet profile, thus validating the previous investigations on synthetic garnets [32], which suggested the relative insensitivity of the pre-edge centroid position to small variations in the $Fe^{3+}/\Sigma Fe$ ratio. To further verify the adequacy of the pre-edge method in determining the Fe oxidation state of the investigated sample, we considered also an alternative approach based on the first moment analysis of the background subtracted pre-edge features [52], which is most often used in the analysis of X-ray emission spectra [53]. Unfortunately, also in this case the calculated first moment energy values do not show a reasonable trend as a function of the position along the garnet profile. Therefore we

should conclude that also this method is not sensible enough in determining the space resolved variation of the $Fe^{3+}/\Sigma Fe$ ratio along the garnet profile.

Berry *et al.* [32] showed that monitoring the absorption edge energy position is a more effective way to estimate the $Fe^{3+}/\Sigma Fe$ ratio in synthetic garnets. In particular they proposed an empirical correlation between the $Fe^{3+}/\Sigma Fe$ ratio and the energy position of the point closest to the 0.9 value of normalized intensity (hereafter $E_{0.9}$). Similar approaches have been used for instance in the speciation of the relative amount of different oxidation states for other transition metals such as Cu^{2+}/Cu^{+} in ethylene oxychlorination catalyst [54-56] or Ni^{2+}/Ni^{0} in doped ZnO thin films [57].

The results of the $E_{0.9}$ method are reported in Figure 4b: the $E_{0.9}$ values obtained for different positions along the garnet profile are significantly different, thus confirming the effectiveness of the $E_{0.9}$ approach also in natural garnets.

In order to quantify the $Fe^{3+}/\Sigma Fe$ ratio variation across our sample, a crucial issue is represented by the reference minerals selected for the calibration procedure. Indeed, quantitative precision improves when the calibration materials are structurally and compositionally similar to the unknowns since the pre-edge feature is sensitive to coordination geometry as well as valence state. Therefore a large set of standards with compositions similar to the investigated sample is required [32]. Unfortunately, such well characterized garnet standards are generally not easily available, thus preventing the routinely application of the micro-XANES technique. However, in our recent paper [30], comparing micro-XANES results with independent electron microprobe "flank method" results, we proved that a satisfactory calibration can be obtained by exploiting a large set of literature data on synthetic Fe^{+3}-bearing garnets. Using the previously calculated calibration line [30], we obtained the quantitative $Fe^{3+}/\Sigma Fe$ ratio variation along the garnet profile reported in Figure 4c. We can notice a progressive decrease in the Fe^{3+} content moving from garnet core to garnet rim, which reflects the different redox conditions experienced by the mineral during its progressive growth at pressure-temperature conditions ranging from 450 °C, 1.7 GPa (garnet core) to 520 °C, 2.6 GPa (garnet rim) [31].

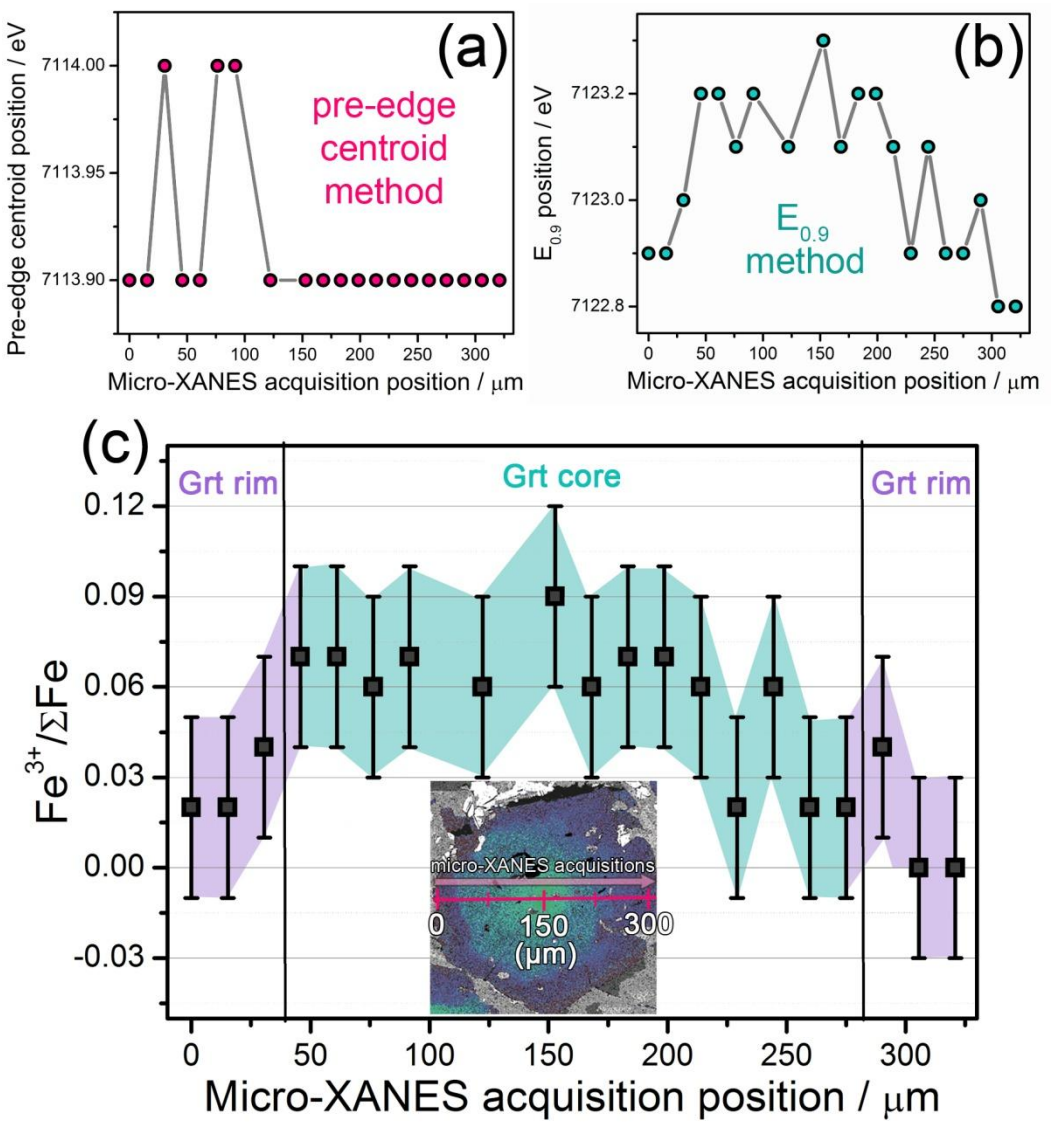

Figure 4. (a) Pre-edge centroid energy position for the Fe K-edge XANES spectra acquired along the magenta line reported in the SEM-EDS map of part (c). (b) As part (a) for the $E_{0.9}$ value. (c) Quantitative spatial variation of the $Fe^{3+}/\Sigma Fe$ ratio obtained from the $E_{0.9}$ values reported in part (b) using a calibration based on a large set of synthetic garnets (see ref. [30]). The error bars on the XANES $Fe^{3+}/\Sigma Fe$ ratios are ± 3% and are calculated by considering the standard deviation of the fit (σ_f = 0.029) and the uncertainty associated with the adopted monochromator energy step (σ_E = 0.1 eV). Although the formal energy resolution of the Si(311) monochromator was 0.5 eV, clear changes where indeed observed, at the Fe K-edge, on the points sampled 0.1 eV apart. In the bottom part an image of the investigated garnet micro-crystal, derived from the processing of major elements X-ray maps acquired at SEM-EDS to visualize the different growth shells, is reported. The sampled profile is highlighted by the magenta line.

3.2 Non-cubic micro-crystals

The analysis of the XANES spectra of non-cubic micro-crystals is more complex since in this case also the X-ray beam polarization has to be taken into account. Despite their still relatively limited number and the difficulties in their interpretation, angle-resolved XAS experiments have contributed to clarify the spectra of transition metals in the pre-edge region [58-63]. Indeed, the angular dependence of polarized spectra may discriminate the dipole transitions from the contributions arising by a quadrupolar mechanism [58, 64, 65]. More in detail, there are three kinds of electronic transitions used to describe the pre-edge features of transition metals compounds which can be distinguished using angle-resolved XAS [65]: (i) 1s → 4p local electric dipole transitions implying the mixing of the empty 3d and p states of the absorbing atom, which is occurring only if the absorbing atom site is not centrosymmetric or if the absorbing atom site centrosymmetry is broken by the atomic vibrations; (ii) non-local electric dipole transition, where the empty p states of the absorbing atom are hybridized with the empty 3d states of the nearest neighbors of the metal via the p empty states of the ligands; (iii) 1s → 3d local electric quadrupole transitions.

Similar polarization effects have been observed in Electron Energy Loss Spectroscopy (EELS) of iron materials and have been extensively studied especially for Fe L-edges [66-68].

It is worth noting that the strong angular dependence of the XANES features for non-cubic single crystals hampers a direct comparison with the more common literature data collected on powdered samples. However, it has been shown that "powder-equivalent" spectra can be obtained by averaging XANES spectra measured for a suitable number of different single crystal orientations [69, 70]. Alternatively, an ideal orientation of the single crystals that provide similar pre-edge peaks as for powdered samples can be found according to the so-called "magic angle" theorem [70].

Figure 5a reports the Fe K-edge XANES spectra of augite and aegirine, which crystallize in the monoclinic system (space groups C2/c), with the beam polarized along two mutually orthogonal directions within the same single crystal. As already observed in previous studies [71, 72], there are two peaks in the main-edge region of the augite spectrum, which are particularly sensitive to the X-ray beam polarization. In particular, in the spectra acquired with the electric field of the X-ray beam oscillating parallel to the [001] crystallographic axis, the intensity of these two features is nearly identical. Moreover, also the position of the pre-edge peak depends on the single crystal orientation.

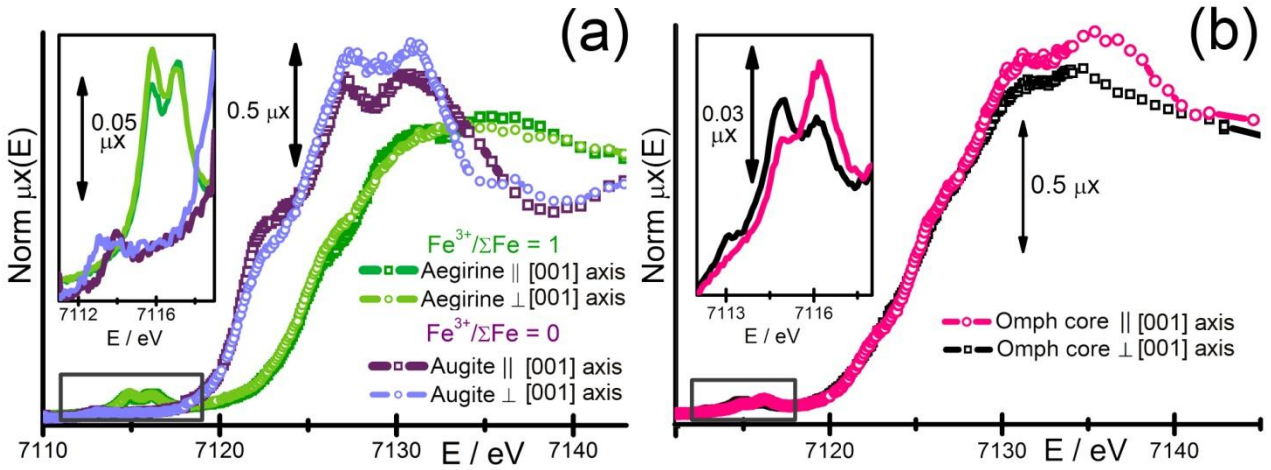

Figure 5. (a) Fe K-edge XANES spectra of aegirine and augite acquired with the X-ray micro-beam polarization parallel (||) and perpendicular (⊥) to the [001] crystallographic axis. (b) As part (a) for the core of an omphacite micro-crystal (Omp_c in Fig. 5b).

For aegirine the position and intensity of the features in the main-edge region is less dependent on the orientation [71]. However, the relative intensity of the two main peak in the pre-edge region (see inset of Figure 4a) can be reversed, passing from a condition when the beam oscillates parallel or perpendicular to the [001] crystallographic axis.

A similar behavior is shown also by the spectra acquired in the core of a zoned omphacite micro-crystal (see inset of Figure 4b), which also crystallizes in the monoclinic system. Also in this case, we can notice a shift towards higher energies of the pre-edge features when the beam oscillates parallel to the [001] crystallographic axis. This observation is not in agreement with previous studies [26, 73], which claimed that the spectral features in the XANES pre-edge region of omphacite do not vary significantly changing the crystal orientation and that, therefore, to a first approximation, the effect of polarization can be neglected for the determination of the $Fe^{3+}/\Sigma Fe$ ratio. Results reported in Figure 4b show that polarization effect can unfortunately not be neglected in this system. This apparent disagreement can be explained by the fact that we used a Si(311) double-crystal monochromator, while the above mentioned investigations employed a Si(111) double-crystal monochromator. Indeed, as clearly shown by Cottrell *et al.* [74], the use of a Si(311) crystal can significantly improve the spectral resolution and thus the accuracy in the oxidation state determination. Indeed, the Darwin width for Si(311) is almost five time sharper than that for Si(111) [1]. It is also worth noting that the studied omphacite micro-crystals are significantly Fe-richer (FeO_{tot} = 8.0 – 14.5

wt%) than those studied by Schmidt *et al.* [26] (FeO_{tot} = 2.8 – 3.5 wt%), thus suggesting that the polarization effect may be hidden at low Fe_{tot} concentrations in the omphacite.

These effects are particularly important when we are in interested in measuring small variations of the $Fe^{3+}/\Sigma Fe$ ratio in micro-crystals with different crystallographic orientations. Figure 5a shows the XANES spectra acquired in the rim and in the core of the same omphacite micro-crystal: these spectra can be directly compared neglecting the polarization effects since the rim and core of the same micro-crystal have the same crystallographic orientation, as highlighted by electron backscatter diffraction (EBSD) analysis. In particular, we can see that the differences in the shape of the pre-edge features due to the slightly different oxidation state of the rim and the core are qualitatively of the same order of magnitude with respect to the variations that can be induced by rotating the sample (Figure 4b). Therefore to accurately determine the small spatial variations of the $Fe^{3+}/\Sigma Fe$ ratio in a quantitative way, as already performed for garnet (see Section 3.1), the effect of the polarization should be taken into account for the measured sample and for the related reference materials.

Further analysis is in progress, involving a polarization-dependent theoretical modeling of the XANES data, to deconvolute the effects separately due to local compositional variations and X-ray linear dichroism phenomena on relevant omphacite spectral features.

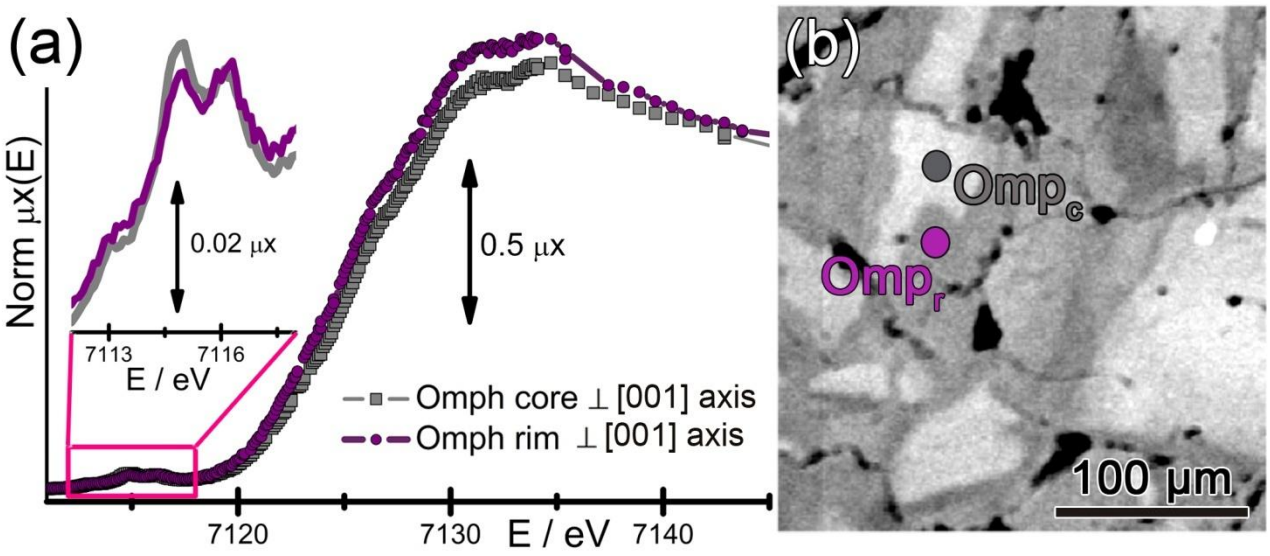

Figure 6. (a) Fe K-edge XANES spectra recorded in the core and rim of the omphacite micro-crystal shown in part (b) (the XANES spectrum of the core is the same reported in Fig. 4b). For both rim and core the X-ray micro-beam polarization was perpendicular (⊥) to the [001] crystallographic axis (b) BSE micrograph of the omphacite micro-

crystals. The violet dot highlights the rim region in which the XANES spectrum reported in part (a) was acquired, while the black dot highlights the core region in which the core spectrum was collected.

4 Conclusions

In this contribution we showed that micro-XANES spectroscopy is a good method for the space resolved determination of the iron oxidation state in complex materials since it does not requires a difficult sample preparation and it allows to collect the spectra *in situ* with a good speed of acquisition.

For cubic Fe-bearing minerals, we discussed two possible methods to calculate the Fe oxidation state based on: (i) the energy positions of the pre-edge centroids; (ii) the energy position of the point closest to the 0.9 value of normalized intensity ($E_{0.9}$). In the case of garnet, we showed that the second approach provides the best results in the investigation of small spatial variations of iron oxidation state at low values of $Fe^{3+}/\Sigma Fe$. In particular, we performed an accurate quantitative analysis of the $Fe^{3+}/\Sigma Fe$ variations in a single zoned micro-crystal of garnet at a high spatial resolution, showing that the $Fe^{3+}/\Sigma Fe$ ratios vary progressively from 0.00 in the garnet rim to 0.09 in the garnet core (see also ref. [30]).

For non cubic micro-crystals, we discussed the effect of the beam polarization on the XANES spectral features. We pointed out that in omphacite the relative intensity of the two main peaks in the pre-edge region can be reversed by changing the crystal orientation with respect to the X-ray beam. Improving the quality of the XANES with respect to previous studies [26, 73] on this mineral, we were able to show that significant modifications in the spectral features in the XANES pre-edge region of omphacite occur when changing the crystal orientation. Hopefully, a more sophisticated analysis will allow us to simulate the polarization effects, also on the basis of the data collected on the reference monoclinic minerals, and thus to quantify the $Fe^{3+}/\Sigma Fe$ across the investigated omphacite micro-crystals.

The analytical procedures discussed in this paper can be easily generalized and employed also for different kind of samples to measure *in situ* their iron oxidation state. This method is consequently relevant in several disciplines such as solid state physics, earth sciences, biology, bio-chemistry and catalysis.

References

[1] S. Bordiga, E. Groppo, G. Agostini, J.A. van Bokhoven and C. Lamberti, Chem. Rev., 113 (2013) 1736.

[2] G. Martinez-Criado, E. Borfecchia, L. Mino and C. Lamberti, in C. Lamberti and G. Agostini (Editors), Characterization of Semiconductor Heterostructures and Nanostructures (Second Edition), Elsevier, Amsterdam, 2013, p. 361.
[3] G.E. Ice, J.D. Budai and J.W.L. Pang, Science, 334 (2011) 1234.
[4] L. Mino, G. Agostini, E. Borfecchia, D. Gianolio, A. Piovano, E. Gallo and C. Lamberti, J. Phys. D: Appl. Phys., (2013) in press.
[5] R. Ortega, A. Carmona, I. Llorens and P.L. Solari, J. Anal. At. Spectrom., 27 (2012) 2054.
[6] J. Chwiej, D. Adamek, M. Szczerbowska-Boruchowska, A. Krygowska-Wajs, S. Wojcik, G. Falkenberg, A. Manka and M. Lankosz, J. Biol. Inorg. Chem., 12 (2007) 204.
[7] S. Yoshida, A. Ektessabi and S. Fujisawa, J. Synchrot. Radiat., 8 (2001) 998.
[8] R. Ortega, G. Deves, S. Bohic, A. Simionovici, B. Menez and M. Bonnin-Mosbah, Nucl. Instrum. Methods Phys. Res. Sect. B-Beam Interact. Mater. Atoms, 181 (2001) 480.
[9] W.M. Heijboer, D.C. Koningsberger, B.M. Weckhuysen and F.M.F. de Groot, Catal. Today, 110 (2005) 228.
[10] S. Hannemann, J.D. Grunwaldt, N. van Vegten, A. Baiker, P. Boye and C.G. Schroer, Catal. Today, 126 (2007) 54.
[11] J.D. Grunwaldt, B. Kimmerle, A. Baiker, P. Boye, C.G. Schroer, P. Glatzel, C.N. Borca and F. Beckmann, Catal. Today, 145 (2009) 267.
[12] J.D. Grunwaldt and C.G. Schroer, Chem. Soc. Rev., 39 (2010) 4741.
[13] A.M. Beale, S.D.M. Jacques and B.M. Weckhuysen, Chem. Soc. Rev., 39 (2010) 4656.
[14] I.L.C. Buurmans and B.M. Weckhuysen, Nat. Chem., 4 (2012) 873.
[15] J.D. Grunwaldt, J.B. Wagner and R.E. Dunin-Borkowski, ChemCatChem, 5 (2013) 62.
[16] E. de Smit, I. Swart, J.F. Creemer, G.H. Hoveling, M.K. Gilles, T. Tyliszczak, P.J. Kooyman, H.W. Zandbergen, C. Morin, B.M. Weckhuysen and F.M.F. de Groot, Nature, 456 (2008) 222.
[17] E. de Smit, I. Swart, J.F. Creemer, C. Karunakaran, D. Bertwistle, H.W. Zandbergen, F.M.F. de Groot and B.M. Weckhuysen, Angew. Chem.-Int. Edit., 48 (2009) 3632.
[18] M. Tada, N. Ishiguro, T. Uruga, H. Tanida, Y. Terada, S. Nagamatsu, Y. Iwasawa and S. Ohkoshi, Phys. Chem. Chem. Phys., 13 (2011) 14910.
[19] J.D. Grunwaldt and A. Baiker, Catal. Lett., 99 (2005) 5.
[20] A. Sakdinawat and D. Attwood, Nat Photon, 4 (2010) 840.
[21] B. Fayard, E. Pouyet, G. Berruyer, D. Bugnazet, C. Cornu, M. Cotte, V. De Andrade, F. Di Chiaro, O. Hignette, J. Kieffer, T. Martin, E. Papillon, M. Salomé and V.A. Sole, Journal of Physics: Conference Series, 425 (2013) 192001.
[22] I.D. Gonzalez-Jimenez, K. Cats, T. Davidian, M. Ruitenbeek, F. Meirer, Y.J. Liu, J. Nelson, J.C. Andrews, P. Pianetta, F.M.F. de Groot and B.M. Weckhuysen, Angew. Chem.-Int. Edit., 51 (2012) 11986.
[23] J.S. Delaney, M.D. Dyar, S.R. Sutton and S. Bajt, Geology, 26 (1998) 139.
[24] M.D. Dyar, J.S. Delaney, S.R. Sutton and M.W. Schaefer, Am. Miner., 83 (1998) 1361.
[25] M.D. Dyar, E.W. Lowe, C.V. Guidotti and J.S. Delaney, Am. Miner., 87 (2002) 514.
[26] R. Schmid, M. Wilke, R. Oberhansli, K. Janssens, G. Falkenberg, L. Franz and A. Gaab, Lithos, 70 (2003) 381.
[27] M. Munoz, V. De Andrade, O. Vidal, E. Lewin, S. Pascarelli and J. Susini, Geochemistry Geophysics Geosystems, 7 (2006).
[28] V. De Andrade, J. Susini, M. Salome, O. Beraldin, C. Rigault, T. Heymes, E. Lewin and O. Vidal, Anal. Chem., 83 (2011) 4220.
[29] G.M. Yaxley, A.J. Berry, V.S. Kamenetsky, A.B. Woodland and A.V. Golovin, Lithos, 140 (2012) 142.
[30] E. Borfecchia, L. Mino, D. Gianolio, C. Groppo, N. Malaspina, G. Martinez-Criado, J.A. Sans, S. Poli, D. Castelli and C. Lamberti, J. Anal. At. Spectrom., 27 (2012) 1725.
[31] C. Groppo and D. Castelli, Journal of Petrology, 51 (2010) 2489.
[32] A.J. Berry, G.M. Yaxley, A.B. Woodland and G.J. Foran, Chem. Geol., 278 (2010) 31.
[33] D. Castelli, Il metamorfismo alpino delle rocce carbonatiche della Zona Sesia-Lanzo (Alpi Occidentali), Unpubl. PhD Thesis, University of Torino, 1987.
[34] D. Castelli and B. Lombardo, Ofioliti, 32 (2007) 1.
[35] A. Somogyi, R. Tucoulou, G. Martinez-Criado, A. Homs, J. Cauzid, P. Bleuet, S. Bohic and A. Simionovici, J. Synchrot. Radiat., 12 (2005) 208.

[36] R. Tucoulou, G. Martinez-Criado, P. Bleuet, I. Kieffer, P. Cloetens, S. Laboure, T. Martin, C. Guilloud and J. Susini, J. Synchrot. Radiat., 15 (2008) 392.
[37] Y. Iketaki, Y. Horikawa, S. Mochimaru and K. Nagai, Jpn. J. Appl. Phys. Part 1 - Regul. Pap. Short Notes Rev. Pap., 35 (1996) 4585.
[38] J.A. Bearden and A.F. Burr, Rev. Mod. Phys., 39 (1967) 125.
[39] B. Ravel and M. Newville, J. Synchrot. Radiat., 12 (2005) 537.
[40] G.W. Flynn and W.J.A. Powell, The Cutting and Polishing of Electro-optic Materials, Adams Hilger, London, 1979.
[41] D.J. Prior, P.W. Trimby, U.D. Weber and D.J. Dingley, Mineral. Mag., 60 (1996) 859.
[42] S. Bajt, S.R. Sutton and J.S. Delaney, Geochim. Cosmochim. Acta, 58 (1994) 5209.
[43] M. Wilke, F. Farges, P.E. Petit, G.E. Brown and F. Martin, Am. Miner., 86 (2001) 714.
[44] G. Giuli, G. Pratesi, C. Cipriani and E. Paris, Geochim. Cosmochim. Acta, 66 (2002) 4347.
[45] A.J. Berry, L.V. Danyushevsky, H.S.C. O'Neill, M. Newville and S.R. Sutton, Nature, 455 (2008) 960.
[46] L.C.C. Ferraz, W.M. Carvalho, D. Criado and F.L. Souza, ACS Appl. Mater. Interfaces, 4 (2012) 5515.
[47] G. Giuli, M.R. Cicconi and E. Paris, Eur. J. Mineral., 24 (2012) 783.
[48] T.E. Westre, P. Kennepohl, J.G. DeWitt, B. Hedman, K.O. Hodgson and E.I. Solomon, J. Am. Chem. Soc., 119 (1997) 6297.
[49] P.E. Petit, F. Farges, M. Wilke and V.A. Sole, J. Synchrot. Radiat., 8 (2001) 952.
[50] A.J. Berry, H.S. O'Neill, K.D. Jayasuriya, S.J. Campbell and G.J. Foran, Am. Miner., 88 (2003) 967.
[51] M. Wilke, G.M. Partzsch, R. Bernhardt and D. Lattard, Chem. Geol., 213 (2004) 71.
[52] H. Visser, E. Anxolabehere-Mallart, U. Bergmann, P. Glatzel, J.H. Robblee, S.P. Cramer, J.J. Girerd, K. Sauer, M.P. Klein and V.K. Yachandra, J. Am. Chem. Soc., 123 (2001) 7031.
[53] E. Gallo, C. Lamberti and P. Glatzel, Phys. Chem. Chem. Phys., 13 (2011) 19409.
[54] C. Lamberti, C. Prestipino, F. Bonino, L. Capello, S. Bordiga, G. Spoto, A. Zecchina, S.D. Moreno, B. Cremaschi, M. Garilli, A. Marsella, D. Carmello, S. Vidotto and G. Leofanti, Angew. Chem. Int. Edit., 41 (2002) 2341.
[55] N.B. Muddada, U. Olsbye, L. Caccialupi, F. Cavani, G. Leofanti, D. Gianolio, S. Bordiga and C. Lamberti, Phys. Chem. Chem. Phys., 12 (2010) 5605.
[56] N.B. Muddada, U. Olsbye, G. Leofanti, D. Gianolio, F. Bonino, S. Bordiga, T. Fuglerud, S. Vidotto, A. Marsella and C. Lamberti, Dalton Transactions, 39 (2010) 8437.
[57] L. Mino, D. Gianolio, F. Bardelli, C. Prestipino, E. Senthil Kumar, F. Bellarmine, M. Ramanjaneyulu, C. Lamberti and M.S. Ramachandra Rao, J. Phys.-Condens. Matter, 25 (2013) 385402.
[58] G. Drager, R. Frahm, G. Materlik and O. Brummer, Phys. Status Solidi B-Basic Res., 146 (1988) 287.
[59] T. SchedelNiedrig, W. Weiss and R. Schlogl, Phys. Rev. B, 52 (1995) 17449.
[60] D. Cabaret, Y. Joly, H. Renevier and C.R. Natoli, J. Synchrot. Radiat., 6 (1999) 258.
[61] A. Marcelli, G. Cibin, G. Cinque, A. Mottana and M.F. Brigatti, Radiat. Phys. Chem., 75 (2006) 1596.
[62] P. Glatzel, A. Mirone, S.G. Eeckhout, M. Sikora and G. Giuli, Phys. Rev. B, 77 (2008).
[63] A. Arcovito, C. Ardiccioni, M. Cianci, P. D'Angelo, B. Vallone and S. Della Longa, J. Phys. Chem. B, 114 (2010) 13223.
[64] C. Brouder, J. Phys.-Condes. Matter, 2 (1990) 701.
[65] D. Cabaret, A. Bordage, A. Juhin, M. Arfaoui and E. Gaudry, Phys. Chem. Chem. Phys., 12 (2010) 5619.
[66] P.A. van Aken and B. Liebscher, Phys. Chem. Miner., 29 (2002) 188.
[67] P.A. van Aken and S. Lauterbach, Phys. Chem. Miner., 30 (2003) 469.
[68] P.S. Miedema and F.M.F. de Groot, J. Electron Spectrosc. Relat. Phenom., 187 (2013) 32.
[69] R.F. Pettifer, C. Brouder, M. Benfatto, C.R. Natoli, C. Hermes and M.F.R. Lopez, Phys. Rev. B, 42 (1990) 37.
[70] M. Munoz, O. Vidal, C. Marcaillou, S. Pascarelli, O. Mathon and F. Farges, Am. Miner., 98 (2013) 1187.
[71] M.D. Dyar, M.E. Gunter, J.S. Delaney, A. Lanzarotti and S.R. Sutton, Canadian Mineralogist, 40 (2002) 1375.
[72] M.C. McCanta, M.D. Dyar, M.J. Rutherford and J.S. Delaney, Am. Miner., 89 (2004) 1685.

[73] M. Terabayashi, T. Matsui, K. Okamoto, H. Ozawa, Y. Kaneko and S. Maruyama, Isl. Arc., 22 (2013) 37.
[74] E. Cottrell, K.A. Kelley, A. Lanzirotti and R.A. Fischer, Chem. Geol., 268 (2009) 167.